Journal of Arid Environments 80 (2012) 45–55

Contents lists available at SciVerse ScienceDirect

Journal of Arid Environments

journal homepage: www.elsevier.com/locate/jaridenv

Monitoring desertification in a Savannah region in Sudan using Landsat images and spectral mixture analysis

M. Dawelbait [a,b], F. Morari [b,*]

[a] Department of Environmental Affairs, Ministry of Environment and Physical Development, Khartoum, Sudan
[b] Dipartimento di Agronomia Ambientale e Produzioni Vegetali, Agripolis, Università di Padova, Viale dell'Università 16, 35020, Legnaro (Padova), Italy

ARTICLE INFO

Article history:
Received 21 December 2009
Received in revised form
15 October 2011
Accepted 22 December 2011
Available online 14 January 2012

Keywords:
Remote sensing
Spectral mixture analysis
Change vector analysis
Landsat
Desertification
Savannah

ABSTRACT

Two Landsat images, acquired in 1987 and 2008, were analyzed to evaluate desertification processes in central North Kurdufan State (Sudan). Spectral Mixture Analysis (SMA) and multitemporal comparison techniques (change vector analysis) were applied to estimate the long-term desertification/re-growing of vegetation cover over time and in space.

Site-specific interactions between natural processes and human activity played a pivotal role in desertification. Over the last 21 years, desertification significantly prevailed over vegetation re-growth, particularly in areas around rural villages. Changes in land use and mismanagement of natural resources were the main driving factors affecting degradation. More than 120,000 km^2 were estimated as being subjected to a medium-high desertification rate. Conversely, the reforestation measures, adopted by the Government in the last decade and sustained by higher rainfall, resulted in low-medium re-growth conditions over an area of about 20,000 km^2.

Site-specific strategies which take into account the interactions of the driving factors at local scale are thus necessary to combat desertification, avoiding any implementation of untargeted measures. In order to identify the soundest strategies, high-resolution tools must be applied. In this study the application of spectral mixture analysis to Landsat data appeared to be a consistent, accurate and low-cost technique to identify risk areas.

1. Introduction

Desertification is defined as land degradation in arid, semiarid and dry sub-humid areas due to climate variation and/or human activity (UNCCD, 1994). The three major land use systems prone to desertification in arid and semiarid areas are rangeland, rain-fed croplands and irrigated lands. Degradation of vegetation cover by overgrazing and the cutting of woody plants for fuelwood, buildings, bush fencing and other purposes is the common desertification process in rangeland (Mustafa, 2007). On rain-fed croplands, wind and water erosion are accelerated by cropland preparation, which involves removal of the native vegetation cover, woodcutting or grass burning. High concentrations of salts in the root zone associated with the introduction of irrigation in dry areas (secondary salinization) have caused desertification due to salts rising with the rise in ground water level (Singh, 2009).

Four aspects must be evaluated in order to render the desertification process measurable (FAO-UNEP, 1984): status, which is defined as the state of a particular piece of land at a specific time compared with its condition in the past; rate, which refers to the change in the condition over time; inherent risk, which is a measure of the vulnerability of landscape to a desertification process; and hazard, which is the overall rating considering the previous three aspects. To make the assessment easier, several Authors have attempted to determine appropriate indicators. Environmental indicators over large areas must be measurable and suitable for regular updating. Few of the proposed indicators are specifically for dryland degradation alone, because it is difficult to separate the effects of climatic factors from those of human activities in such areas (Diouf and Lambin, 2001; Mabbutt, 1986; Rubio and Bochet, 1998).

Difficulties have also arisen because the interpretation of the UNCCD desertification definition can differ greatly according to the choice of indicators. Soil erosion and sedimentation, perennial plant cover and biomass have been used as indicators of the desertification status (Le Houerou, 2006). However a recent survey among 90 experts has recognized the long-lasting loss of vegetation cover and productivity over time and in space as the key indicator/variable of desertification (Hellden, 2008).

* Corresponding author. Tel.: +39 0498272857; fax: +39 0498272839.
E-mail address: francesco.morari@unipd.it (F. Morari).

0140-1963/$ – see front matter © 2011 Elsevier Ltd. All rights reserved.
doi:10.1016/j.jaridenv.2011.12.011

One of the most effective tools for desertification assessment is remote sensing. It has long been suggested as a time and cost efficient method for observing dryland ecosystem environments (Hassan and Luscombe, 1990), monitoring land cover degradation, as well as characterizing the dynamism of sand dunes (Collado et al., 2002).

Most remote sensing in arid regions has concentrated on optical remote sensing techniques which use data from sensors that collect radiation in the reflected solar spectrum. Two main approaches are usually followed (Dawelbait and Morari, 2008; Smith et al., 1990): a) calculation of vegetation indices; b) image classification.

A relationship between plant biomass and a standardized vegetation index can be established (Tucker, 1979). Vegetation indices, reviewed by Jackson et al. (1983), Tueller and Oleson (1989) and others, are generally based on ratios of the radiance in the red and infrared spectral bands, chosen to maximize the reflectance contrasts between vegetation and other materials. The Normalized Difference Vegetation Index (NDVI) has been most commonly used to map spatial and temporal variation in vegetation (Tucker, 1979). NDVI is sensitive to pixel-level changes in greenness and fraction of photosynthetically active radiation absorbed but is not differentially sensitive to change in vegetation cover versus vegetation condition (i.e. the vigour, photosynthetic capacity or stress of vegetation canopy or cluster). This means that when an NDVI change occurs, it cannot be readily determined whether or not it was caused by altered vegetation cover or condition of cover (Asner, 2004). Moreover, NDVI has only limited success in providing accurate estimates of shrubland cover in arid areas and limited utility in an arid ecosystem. This is due to spectral variability of background materials such as soil and surface litter and the strength and variation of soil spectral albedo, which causes nonlinearity in the relationship between NDVI and vegetation characteristics (Asner, 2004; Huete, 1988; Huete et al., 1992).

Image classification usually relies on statistical methods including maximum-likelihood, clustering and discrimination analysis or methods based on principal components analysis (PCA) (Smith et al., 1990). PCA is used to identify a change in heterogeneity. However, to obtain an accurate measurement the pixel size must be smaller than the scale of variability of at least one of the principle landscape elements (e.g. grasslands).

Spectral mixture analysis (SMA) is a sub-pixel classification technique which could be use to unmix the soil-plant canopy measurements into the respective soil, vegetation, and non-photosynthetic vegetation (Smith et al., 1990). SMA depends on the spectral response of land cover components. The spectral response in remote sensing from open canopies is a function of the number and type of reflecting components, their optical properties and relative proportions (Adams et al., 1995). SMA appears to be the most efficient technique to obtain information on vegetation cover, soil surface type and vegetation canopy characteristics in semiarid areas because the scale of variability of the principle landscape elements in semiarid areas is larger than the pixel size in most of the remote sensing satellite imageries (Adams et al., 1995; Dawelbait and Morari, 2008; Okin and Robert, 2004).

Sudan is a developing country where desertification is widespread. UNEP considers that three compounding desertification processes are underway (UNEP, 2007): climate-based conversion of land types from semi-desert to desert, mainly due to a reduction in annual rainfall; degradation of existing desert environments, including wadis and oases, principally caused by deforestation, overgrazing and erosion; conversion of land types from semi-desert to desert by human action (deforestation, overgrazing and cultivation) even if rainfall may still be sufficient to support semi-desert vegetation. These processes are relatively difficult to distinguish, separate and quantify on the ground (Diouf and Lambin, 2001).

Specific studies are therefore necessary in order to define the driving variables affecting the processes and adopt efficient site-specific strategies to combat desertification. Since limited funds are provided to Sudanese research institutions, remote sensing can be a reliable tool to study desertification without incurring high costs (e.g. Ali and Bayoumi, 2004; Dafalla and Casplovics, 2005; Khiry, 2007).

This paper aimed to a) test the application of SMA to Landsat images as a tool to study the desertification phenomenon and b) individuate and quantify the driving variables influencing land degradation in a savannah region in the central part of Sudan.

2. Material and methods

2.1. Study site

The study site is located in the north of Umrowaba in North Kordodan State, central Sudan, in the Sahelian eco-climatic zone (between latitude 12°56′35″ and 13°3′49″N and longitude 31°0′51″ and 31°58′51″ E) (Fig. 1). The climate is semiarid with annual rainfall ranging from 200 to 750 mm, concentrated during a few summer months (June to September/October), with a peak in August. Mean annual temperature is about 20 °C, but the daytime temperature can rise as high as 45 °C during summer.

The soil is a Cambric Arenosols (FAO-UNESCO, 1997), coarse sandy, of Aeolian origin with high infiltration rates and inherent low fertility. Sand sheets and sand dunes stabilized by vegetation are the main natural formations. Natural vegetation consists of trees (*Acacia* spp.), bushes and grass, *Aristida pallida* Steud. on crests of dunes, *Eragrostis termula* Tnismert. in the troughs and *Cenchrus biflorus* Roxb., which grows after crop cultivation. Rangeland and rain-fed croplands are the most important land use systems. The main crops are sorghum (*Sorghum vulgare* Pers.), millet (*Panicum miliaceum* L.), sesame (*Sesamum indicum* L.) and watermelon (*Citrullus lanatus* (Thunb.) Matsum & Nakai). The rainy season usually leads to a short growing period (from June to October) followed by a long dry season with a reduction in green vegetation. The peak of biomass is observed at the end of the rainy season (September–October).

2.2. Data acquisition and preprocessing

Landsat Thematic Mapper (TM5) and Landsat Enhanced Thematic Mapper plus (ETM+7) scenes acquired on September 15th 1987 (TM5 Sep 15) and October 18th 2008 (ETM+7 Oct 18) were analyzed. The dates coincided with the end of the rainy season and were selected for monitoring the potential long-term processes of desertification, since both of them were acquired in periods of comparable rainfall amount (5 mm in September 1987 and 8 mm in October 2008) even considering the antecedent months (e.g. 113 in August 1987 and 92 mm in August 2008).

Landsat images were selected because they are free of charge, with high monitoring frequency and cover areas appropriate for monitoring the environment in a large geographic zone. Landsat TM5 and ETM+7 have a temporal revisit time of 16 days and a spatial resolution of 30 m with six visible/near infrared bands and one thermal band. The gaps in ETM+7 scan-line corrector (SLC)–off were filled using the localized linear histogram mach (LLHM) method (Scaramuzza et al., 2004). Landsat 7 ETM + SLC − off, November 3rd 2008 was used to fill the gaps since the time lag between the two images was only 15 days and the gaps were not overlapping.

ETM+7 Oct 18 was co-registered to TM5 Sep 15 to undertake comparative analysis. Images were not referenced to a standard

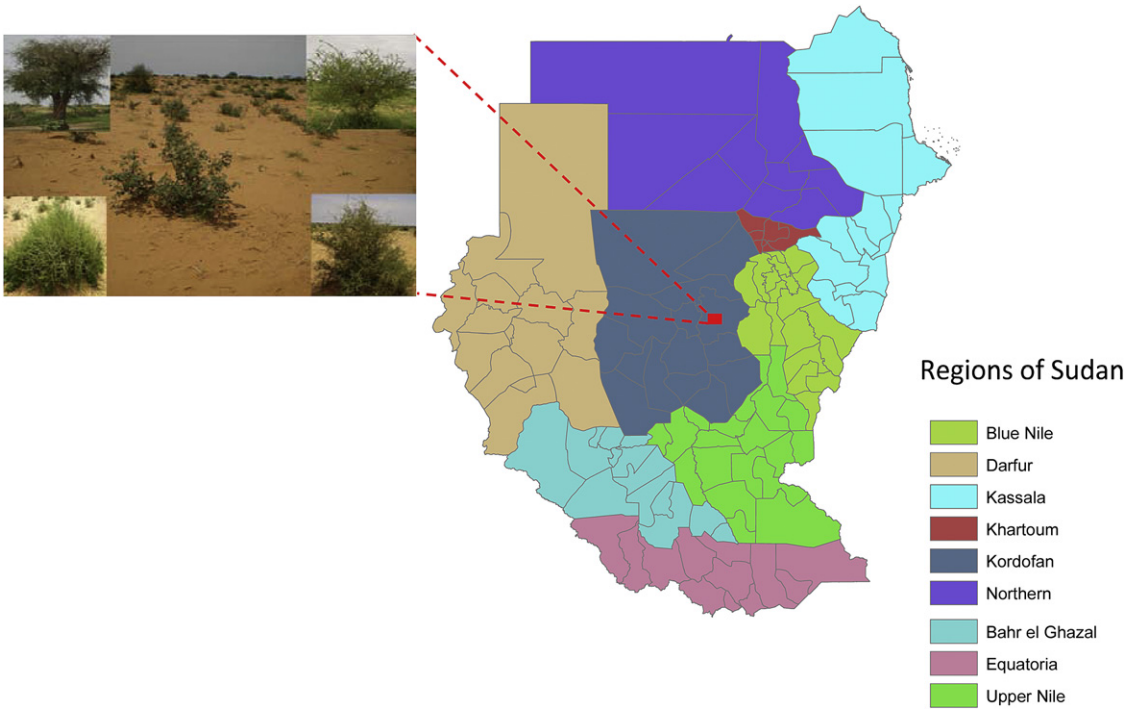

Fig. 1. Study site position and main landscape elements.

map base, since the only available map had a coarser resolution (scale 1:250,000). They were geometrically rectified using 13 ground control points to accurately mach them to ground reference data. The nearest neighbour assignment (Lillesand et al., 2004) was applied yielding a root mean square (RMS) error of 0.34 pixels. Subsets covering only the study area were then extracted from each image. To apply SMA the digital number (DN) of the images band1-5 and 7 recorded in 8 bits were converted to exo-atmospheric reflectance units according to Markham and Barker, (1986). The conversion also improved the image quality (De Asis and Omasa, 2007). No atmospheric correction techniques, such as empirical line calibration (Moran et al., 2001) or dark object subtraction (Chavez, 1988) were applied since they have no significant effect on the modelling (Wu, 2004).

2.3. Spectral mixture analysis

In remote sensing images of arid and semiarid environments, the pixel contains mixed spectral information due to the high variability in the distribution of land cover components. SMA is based on the concept that the variance across a given scene is dominated by the relative proportion of a few spectrally distinct components (Elmore et al., 2000). SMA transforms radiation or reflectance data into fractions of a few dominant endmembers, which are fundamental physical components of the scene and not themselves a mixture of other components (Elmore et al., 2000). Fraction images represent the mixing proportions of these endmember spectra (Adams et al., 1986; Smith et al., 1985). SMA generally involves three steps (Huete, 2004): a) assessment of dimensionality or number of unique reflecting materials in a landscape to obtain the endmembers; b) identification of the physical nature of each endmember within a pixel; c) determination of the amounts of each endmember in each pixel.

The basic linear spectral mixture analysis (LSMA) equation is (Okin and Robert, 2004):

$$R_P(\lambda) = \sum_{i=1}^{n} f_i R_i(\lambda) + \varepsilon(\lambda) \quad [1]$$

Where $R_p(\lambda)$ is the apparent surface reflectance of a pixel in an image, f_i is the weighting coefficient ($\sum_{i=1}^{n} f_i = 1$) interpreted as fraction of the pixel made up of the endmember $i = 1,2 \ldots n$, $R_i(\lambda)$ is the reflectance spectrum of spectral endmember in an n-endmember model and $\varepsilon(\lambda)$ is the difference between the actual and modelled reflectance. f_i represents the best fit coefficient that minimizes RMS error given by the following equation:

$$\mathrm{RMS} = \left[\frac{\sum_{j=1}^{m} (\varepsilon_j)^2}{m} \right]^{0.5} \quad [2]$$

where ε_j is the error term for each of the m spectral bands considered.

One problem related to the application of SMA is nonlinear mixing, which can hinder the SMA applications (Ray and Murray, 1996; Roberts et al., 1993). Nonlinear mixing occurs when photons interact with more than one type of object on the earth before returning to the sensor (Asner, 2004). However, the importance of the effect is not widely recognised since other studies (Qin and Gerstl, 2000; Villeneuve et al., 1998) showed that nonlinear mixing is a secondary feature.

2.4. Endmembers

Some SMA approaches use endmember spectra derived from the image (image endmember) (e.g. Elmore et al., 2000; Wessman et al., 1997), whereas others employ libraries of endmember spectra (library endmember), which are produced from reflectance measurement in a laboratory (e.g. Smith et al., 1990). Tompkins et al. (1997) pointed out that endmembers selection is the most critical step in SMA to provide a physically meaningful fraction. While library endmembers would undoubtedly represent a purer

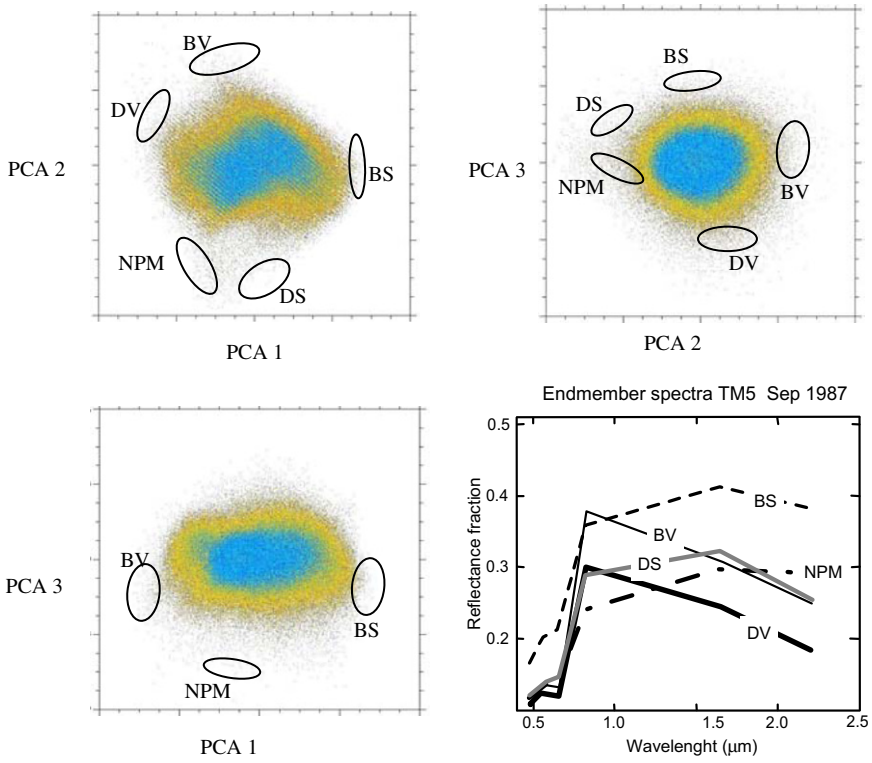

Fig. 2. Scatter plot of the first three PCs and location of the five endmembers (a,b,c); endmember spectra (d).

endmember spectrum and would possibly have given a more accurate absolute abundance, image endmembers simply produce a different scaling and can thus be used for change detection (Elmore et al., 2000). Bateson and Curtiss (1996) and Bateson et al. (2000) generated SMA models using PCA to explore image data in multiple dimensions, although in drylands it is exceedingly difficult to locate image pixels containing 100% cover of each appropriate endmember. One advantage of this technique is that the selection of the endmember spectra is based on inherent spectral variability of the image data without requiring homogeneous pixels of each endmember (Asner, 2004). The approach of Johnson et al. (1985) and Smith et al. (1985) was used to select the endmembers in this paper. The method is based on PCA application to identify the individual endmembers of multiple surface components. The authors observed that for a mixture of three substances (e.g. minerals) the scatter plot of the first two principle components produced a triangle in which the 'pure' endmembers were located at the corners. Several studies have adapted this technique by analyzing different principal component pairs and have managed to successfully obtain image endmembers within different environments (Brandt and Townsend, 2006; Drake and White, 1991; Small, 2001, 2004; Theseira et al., 2003). The use of limited spectral resolution of broadband multispectral sensors such us Landsat ETM+, however, does not permit to distinguish materials with similar but distinct surface reflectance (Small, 2004). In this sense each spectral endmember may represent an aggregate of land cover types (Small, 2004).

In this study a PCA was applied to Landsat images using ENVI to identify endmembers. The spectral mixing space as represented as orthogonal scatterplots of the first three PC bands were generated and the vertices of these plots were selected as endmembers after visualization in the original images. Endmember spectra were applied to SMA in order to produce the fraction images with associated the RMSE images. All image processing was performed within the ENVI remote sensing image analysis environment (ITT Visual Information Solutions).

2.5. Change detection

Long-term variation in land use and land cover (LULC) was obtained by calculating the difference in fraction images applying map-algebra and Change Vector Analysis (CVA) (Kuzera et al., 2005; Malila, 1980). CVA allows the direction and magnitude of change between two time periods to be evaluated. The bright vegetation (BV) and bright soil (BS) fraction images were used to monitor the vegetation re-growing and desertification between 1987 and 2008.

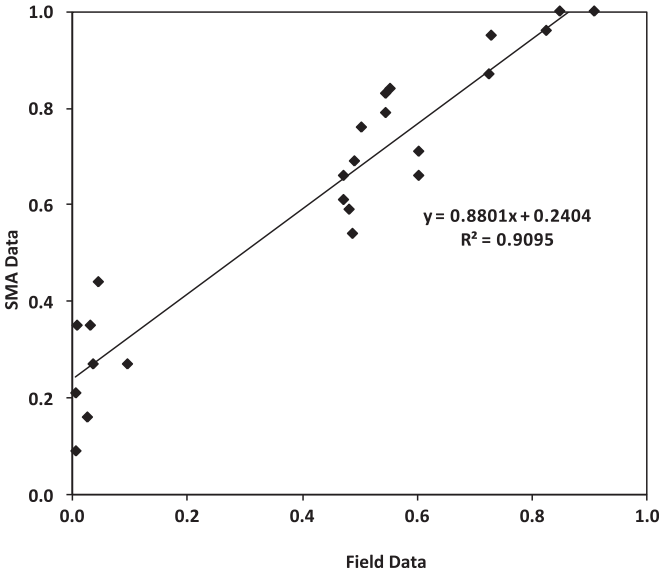

Fig. 3. Scatter plot correlation between measured and SMA estimated vegetation fraction in 2008.

The magnitude of vector change (R) was calculated as follow:

$$R = \sqrt{(BS_1 - BS_2)^2 + (BV_1 - BV_2)^2} \quad [3]$$

where the subscript 1 and 2 indicate the fraction covers in 1987 and 2008

Change direction was measured as the angle (α) of the change vector from a pixel measurement in 1987 to the corresponding pixel in 2008 according to:

$$\tan\alpha = \frac{(BS_1 - BS_2)}{(BV_1 - BV_2)} \quad [4]$$

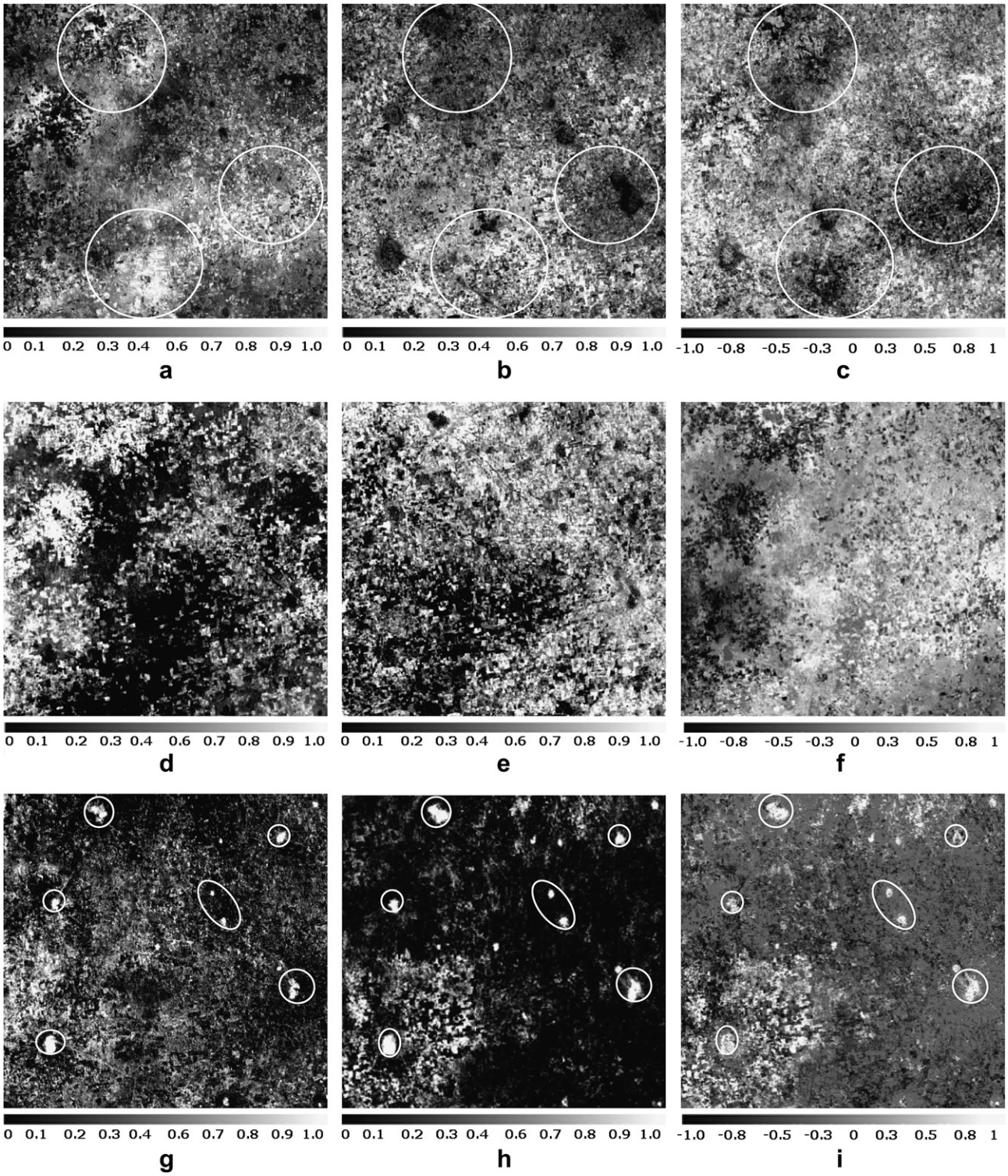

Fig. 4. BV, BS and NPM fraction images and change detection in long-term monitoring: (a) BV in 1987, (b) BV in 2008, (c) difference in BV, d) BS in 1987, (e) BS in 2008 (f) difference in BS, (g) NPM in 1987, (h) NPM in 2008 and (i) difference in NPM. Circles in (a), (b) and (c) indicate the three main areas affected by desertification; circles in (g), (h), (i) indicate the rural villages and their expansion over 21 years.

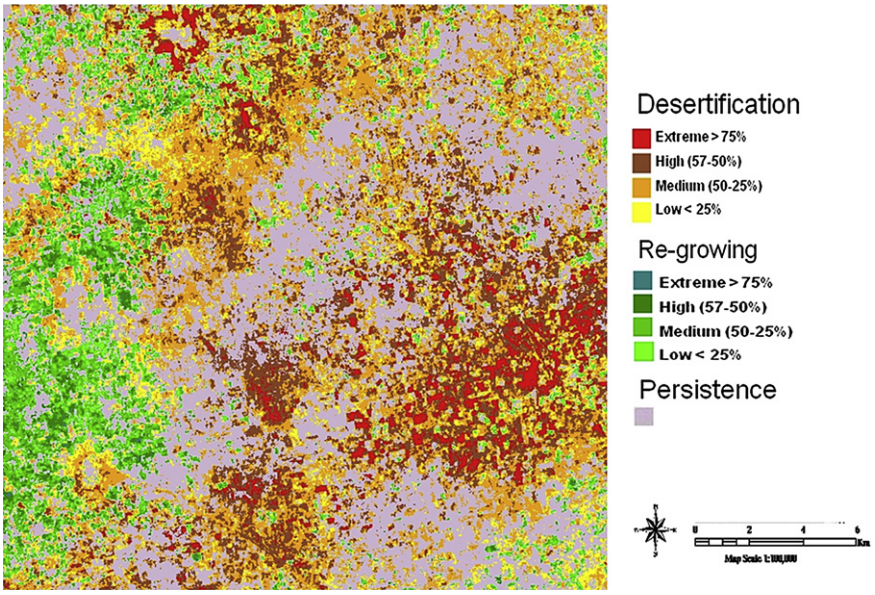

Fig. 5. Desertification and re-growth areas calculated by applying change vector analysis.

Angles measured between 90° and 180° indicated an increase in BS and decrease in BV, and therefore an increase in desertified area. On the contrary, angles measured between 270° and 360° indicated a decrease in sand and an increase in vegetation and therefore represented re-growth conditions. Angles measured between 0°–90° and 180°–270° indicated either increase or decrease in both BV and BS, and consequently persistence in the conditions (Khiry, 2007). Change of magnitude is measured as the Euclidean distance or length of the change vector from a pixel measurement in 1987 to the corresponding pixel in 2008. Four classes of magnitude were represented for either desertification or re-growing according to Kuzera et al. (2005).

2.6. Field survey

A 2-weeks field survey was conducted in October 2008 in order to test the accuracy of SMA using ground vegetation data as references. A total of 16 mixed ground cover plots (size 60 × 60 m for each plot) were selected. Vegetation was composed of a mixture of acacia trees, bushes, grass and shrubs. Trees and bushes were georeferenced with a GPS and the crown diameters were measured and orthogonally projected to the ground surface to estimate the percentage cover. The percentage cover of grass and shrubs was estimated using the line point intersect sampling method (Elmore et al., 2000). The method consists of horizontal, linear, measurements of plant intercepts along the course of a line. The percent cover of each plant species is obtained by totalling the intercept measurements for all individuals of that species along the transect line and converting this total to a percent. Measurements of the grass and shrubs were taken along 30 60-m long transects, oriented in N–S direction, every 2 m. Measurement points were selected at 60 cm intervals along the transect.

The accuracy of SMA was estimated by scatter plot correlation comparing total percentage of live cover in each plot with the live cover (vegetation) fraction image.

3. Results and discussion

3.1. Endmember spectra and SMA applications

The PC analysis of TM5 Sep 15 data found that the first three components explained over 99% of the variance and that simulated data were mean-corrected and projected onto the space determined by those components. In this PC-reduced space five endmembers were manually selected (Fig. 2): bright vegetation (BV), dark vegetation (DV), bright soil (BS), dark soil (DS) and non-photosynthetic material (NPM). BV consisted of all types of natural vegetation (e.g. dense shrubs, grass) and cultivated crops with higher leaf chlorophyll and water content. DV consisted of natural vegetation with lower leaf chlorophyll/water content (senescing vegetation). NPM identified villages (e.g. straw houses), dormant trees and senesced grass and shrubs. BS and DS represented coarse sandy soils and fine sandy soils with higher organic matter in the top layer, respectively. A higher soil organic matter content usually also implies a higher soil water holding capacity and subsequently higher water content. The

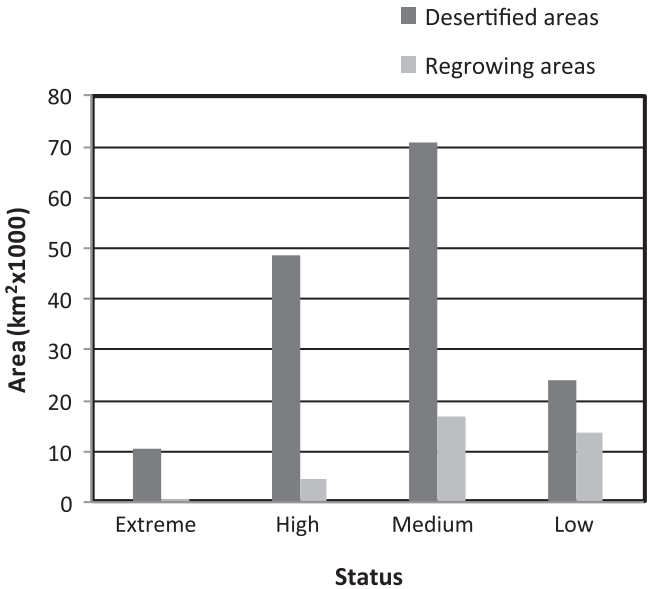

Fig. 6. Classification of study site according to the desertification and re-growth magnitude classes.

effect of shadow was ignored since it is reduced for the sparse canopies typical of many semiarid bush species (Trodd and Dougill, 1998). Endemembers were identified according to the criterion of the minimally inclusive feature space selection (Small, 2001). The minimally inclusive endmembers were averages of smaller numbers (c.a. 90) of reflectance profiles corresponding to the pixels nearest to the apexes of the scattergram. Once the image endmembers were determined their relationship to physically meaningful target have been established. Anyway, not all image components can be effectively modelled using simple endmember models (Brandt and Townsend, 2006). The endmember set was selected to maximize the model performance for BV, and BS which is more vulnerable to wind erosion than DS. To find the best quality of fraction images, three combinations of endmembers were tested (Lu and Weng, 2004). The combinations were: 1) all five endmembers; 2) four endmembers with BV, NPM, BS and DS; 3) three endmembers with BV, NPM, and BS. Fraction images derived from different combinations of endmembers were evaluated with visual interpretation, error extent and distribution in the error fraction image. The combination with four endmembers (BV, NPM, BS and DS) was chosen since it provided the best distinction of LULC types and lowest errors.

The set of endmember spectra selected on TM5 Sep 15 was therefore used also on ETM+7 Oct 18. Using the identical endmembers to analyze multitemporal images strengthened the change analysis (Elmore et al., 2000). Similar to using reference endmembers from a spectral library, using identical image endmembers for different images allows a direct comparison of resulting endmember proportions (Brandt and Townsend, 2006). The RMS error images for SMA process ranged from 0% to 3% for TM5 Sep 15 and from 0% to 2.8% for ETM+7 Oct 18.

Fig. 3 shows the scatter plot correlation between the percentage of vegetation determined with SMA (ETM+7 Oct 18) and field data. In general, the correlation between them is good with an R^2 of 0.91 but with a slight overestimation, especially at lower SMA values. Similar results were obtained by Small (2001) estimating the vegetation abundance of an urban environment using Landsat TM data. A three-component (high albedo, low albedo and vegetation) linear mixing model provided consistent estimates of vegetation fraction but only for values higher than 0.2. There are three main sources of error that could have affected the comparison. The first one can be due to the misregistration of multidate scene and location of the field sites. This is potentially the largest source of error (Elmore et al., 2000), especially in our case where the geometric rectification

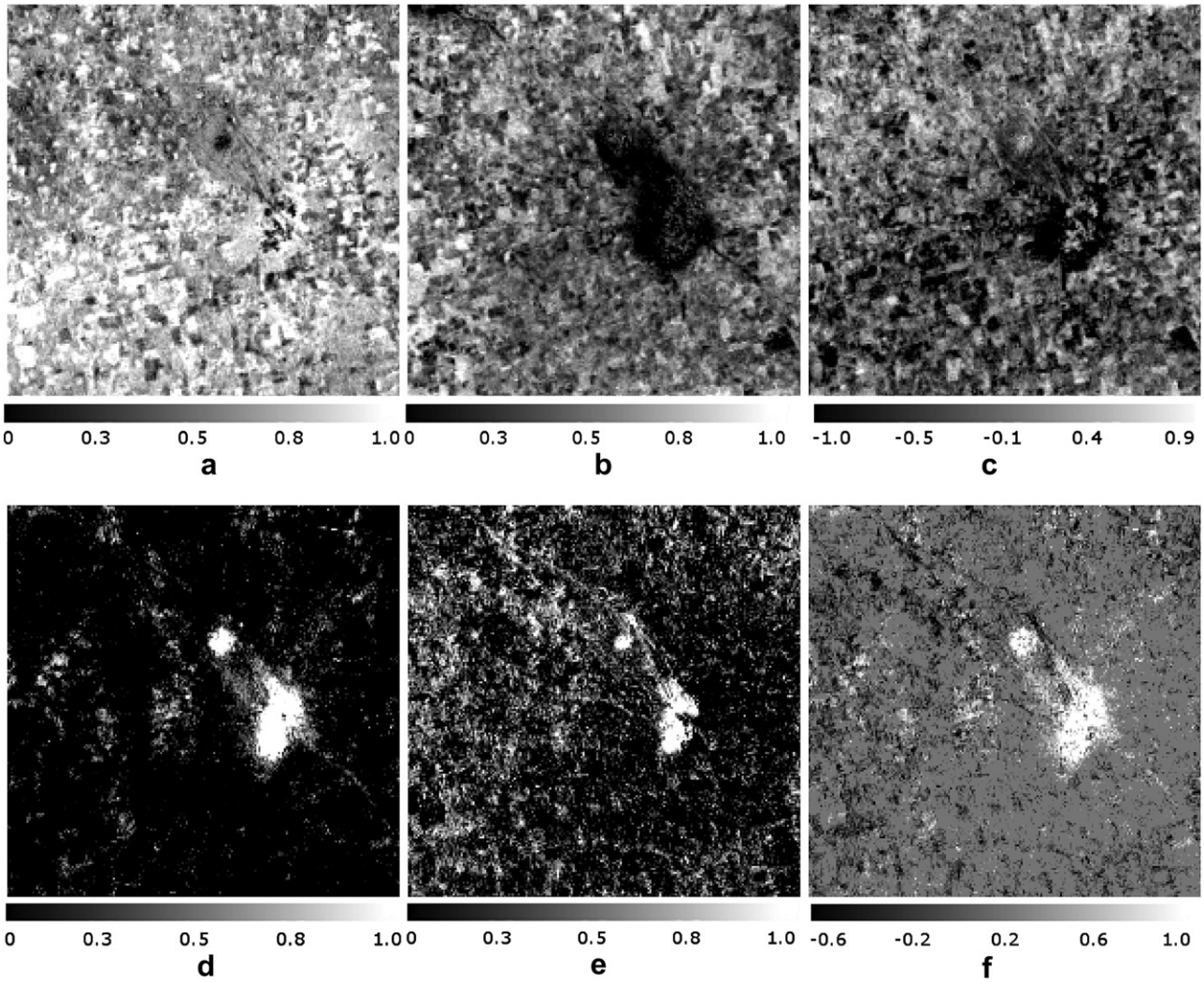

Fig. 7. Detailed views of the degraded eastern part of the site: (a) BV in 1987, (b) BV in 2008, (c) difference in BV, (d) NPM in 1987, (e) NPM in 2008 and (f) difference in NPM. The expansion of the village is clearly shown by two large clusters of pixels with value 1 in (f).

was done with 13 ground control points for all the scenes before subsetting of the study area. This was done because the study area had no fixed sharp points that could be used as control points. Moreover, most of the sites were characterized by a higher degree of scene heterogeneity that could have increased the uncertainty in location (Elmore et al., 2000). Other sources of error can be related to the application LLHM method error to fill the gaps in ETM+7 Oct 18 (Scaramuzza et al., 2004) and accuracy of the field survey, especially in the estimation of grass and bushes. Considering the comparative approach of the present work, the overestimation errors were considered acceptable to evaluate the LULC change.

3.2. Change detection

SMA was performed to determine the relative proportions of BV, BS, DS and NPV for each satellite image (Fig. 4). High abundance of each endmember is indicated in the figures by brighter pixels whereas low abundance is indicated by darker pixels.

Images analysis clearly indicates the existence of heterogeneous and contrasting conditions within the study site. Relevant negative variations in BV fraction (<-0.1) were observed mainly in three large areas, located near rural villages. In the first two, one in the north and the other in the south, the average change in BV was -0.1 and -0.16 respectively. The eastern part spreads over a larger surface area, with an average change in BV fraction of -0.2.

According to CVA (Fig. 5), the magnitude of desertification ranges from low to extreme, with a prevalence of severe degradation conditions (high or extreme) in the eastern part. Change detection analysis also shows the existence of re-growth conditions, mostly spread in the south-western part. Overall, desertification prevailed over re-growth, (Fig. 6) affecting an area of 153,867 km^2, with a prevalence of medium (70,944 km^2) and high (48,578 km^2) classes of magnitude. Re-growth was estimated on an area of 35,313 km^2, mainly classified as medium (17,005 km^2) and low (13,708 km^2). However, average estimation is not sufficient to provide a clear representation of driving factors of change at landscape scale (Anyamba and Tucker, 2005; Collado et al., 2002).

The degradation was driven by various factors, which operated with different intensity in the areas. In the eastern part the expansion of villages triggered the change in land use and mismanagement of the natural resource, mainly caused by deforestation to supply wood for domestic uses i.e. building, cooking, etc., and overgrazing (Sherbinin, 2002). More details of the dynamism around villages are given in Fig. 7. The NPV fraction change image shows two large patches of pixels with value 1

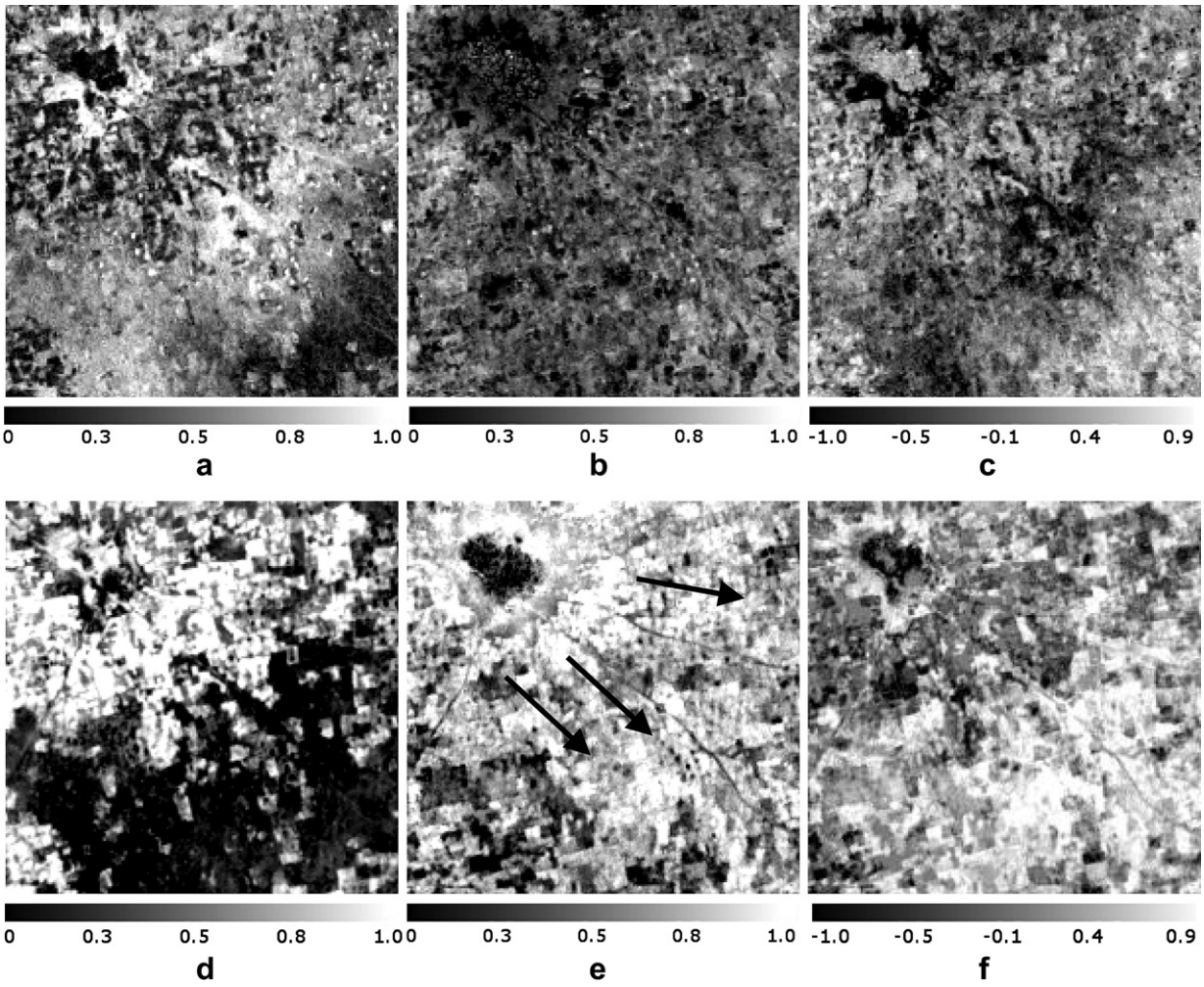

Fig. 8. Detailed views of the degraded northern part of the site: (a) BV in 1987, (b) BV in 2008, (c) difference in BV, (d) BS in 1987, (e) BS in 2008 and (f) difference in BS. Figures clearly illustrate the effect of sand movement according to the prevailing wind directions (arrows).

(new straw houses) due to the expansion of the village over 21 years.

Two other processes affecting soil degradation were recognized by SMA. The first one is related to sand exposure. In the northern area a sand dune (locally called Gouz) is visible in the BS fraction image of 1987, along the SE borders of the village of Tafantara (Fig. 8). At that time, the dune was stabilized by natural vegetation but deforestation for domestic purposes and overgrazing caused the degradation of the site. The change in BV fraction clearly demonstrates the magnitude of the process (Fig. 8). The degradation led to the exposure of the sand dune in an E-SE-S direction according to the prevailing wind direction in winter and early summer (Fig. 8).

The conversion of rangeland into cultivated croplands is the third phenomenon that could have affected the desertification of the study site. In the southern part (Fig. 9), the BV fraction in 1987, on average 0.46, was represented mainly by rangeland. At the same time the average BS fraction was 0.1. The change in land use to cultivation led to a decrease in BV, especially in the central part and a contemporary massive increase in BS fraction. It is not sure that in all zones changes in land use lead necessarily to desertification, since an increase in BS fractions could also be associated to post-harvest field surface conditions. However in general the conversion of dry and fragile rangelands into traditional and mechanized cropland has already been indicated by many Authors as one of the main processes affecting desertification in Sudan e.g (Ayoub, 1998; UNEP, 2007). Over-exploitation of semi-desert environments through deforestation, overgrazing and cultivation results in habitat conversion to desert, even though rainfall may still be sufficient to support semi-desert vegetation (Nicholson, 2005).

Re-growth conditions observed in the SW part were mainly due to Government reforestation projects in last decade and sustained by higher rainfall in the last years in the study area. The Rainfall Anomaly Index (RAI) (Tilahun, 2006) time series (Fig. 10) confirmed the existence of favourable conditions for vegetation growth from the 1990s to 2008, with higher frequency of positive anomalies than in the 1970s and 1980s.

This result is in accordance with the recent satellite and model based studies of the Sahel (e.g. Anyamba and Tucker, 2005; Eklundh and Olsson, 2003), which demonstrated that vegetation has recovered from the peak drought conditions suffered in the region in the 1980s. For example, Anyamba and Tucker (2005), monitoring the Sahelian vegetation dynamics using NDVI in the period 1981–2003, observed the prevalence of greener than normal conditions from the 1990s to 2003. Indeed, NVDI time series followed a similar increase in rainfall over the region during the last decade and indicates a gradual slow but persistent recovery from the 1980s.

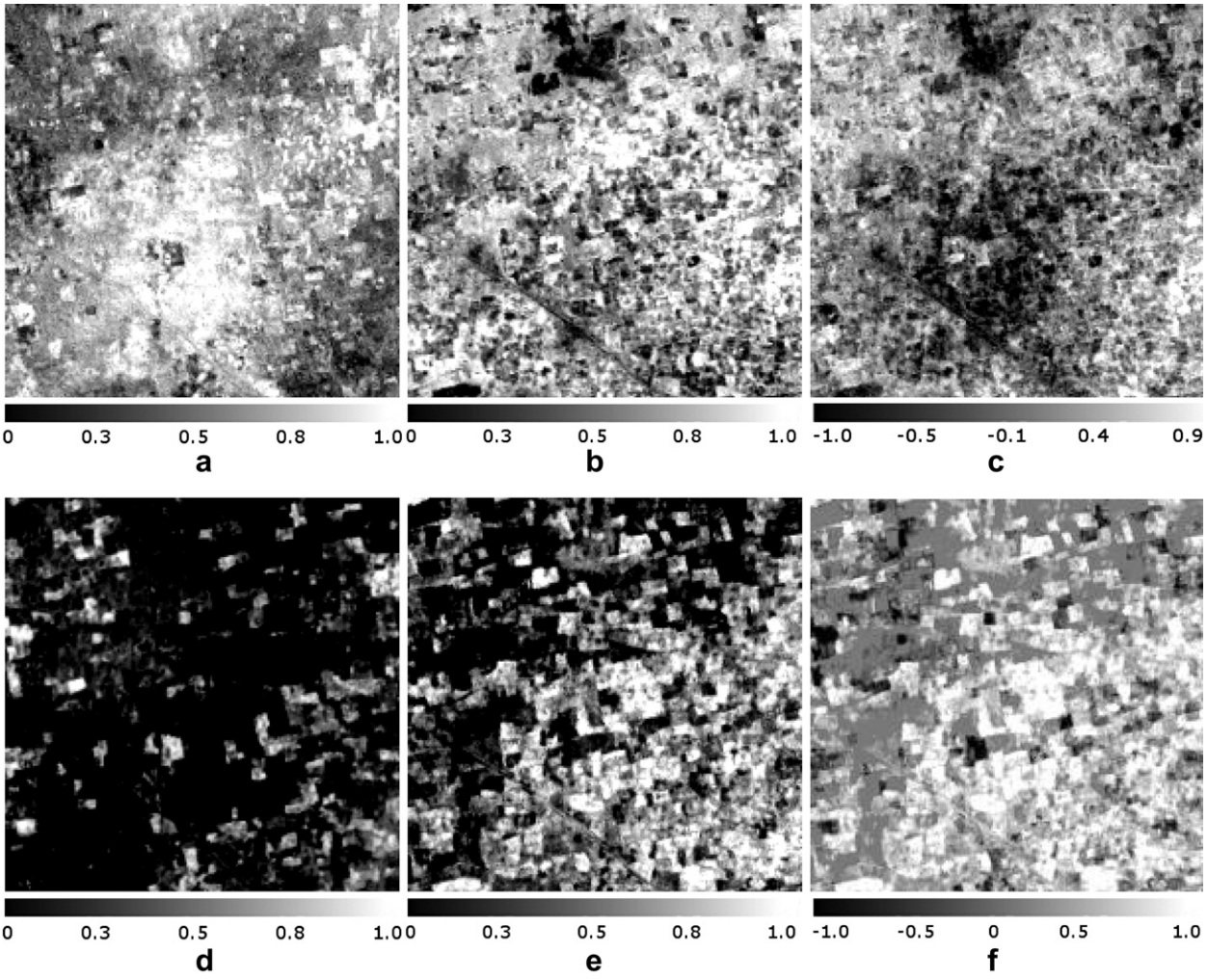

Fig. 9. Detailed views of the degraded southern part of the site: (a) BV in 1987, (b) BV in 2008, (c) difference in BV, (d) BS in 1987, (e) BS in 2008 and (f) difference in BS.

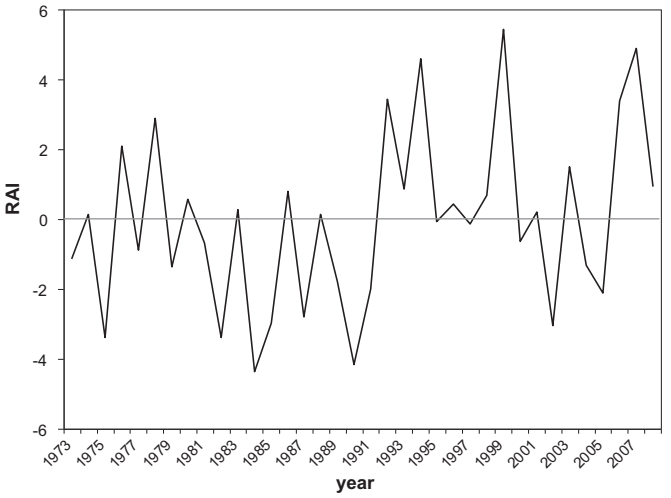

Fig. 10. Rainfall Anomaly Index (RAI) from 1973 to 2008.

4. Conclusions

Site-specific interactions between natural processes and human activity play a pivotal role on desertification in North Kordodan State. Even if phenomena at large scale (e.g. positive rainfall trend) in the last years have allowed a gradual recovery from the peak drought conditions suffered in the Sahel during the 1980s, there are still forcing variables that act at local scale to cause land degradation. One of the most important factors affecting such degradation is human activities, which exploit the natural resources beyond their ecological resilience threshold until desertification is irreversible (Hellden, 2008). Hunger and local energy needs seem to be the driver of land use and management.

Site-specific strategies that take into account the interactions of the driving factors at local scale are thus necessary to combat desertification, avoiding the implementation of untargeted measures. In order to identify the soundest strategies, high-resolution tools must be applied. In this study, the application of spectral mixture analysis to Landsat data appeared to be a consistent, accurate and low-cost technique to obtain information on vegetation cover, soil surface type, and identify risk areas.

Acknowledgements

Research scholarship of Mona Dawelbait was provided by the Ministry of Foreign Affairs – Italy (D.G.C.S). Authors acknowledge Dr. Abdallah Jaafar and Hatim Mukhtar Elnour, National Forest Corporation – Sudan, for their support in the field survey.

References

Adams, J.B., Smith, M.O., Johnson, P.E., 1986. Spectral mixture modeling: a new analysis of rock and soil types at the Viking Lander I Site. Journal of Geophysics Researches 91, 8098–8112.

Adams, J.B., Sabol, D.E., Kapos, V., Almeida-Filho, R., Roberts, D.A., Smith, M.O., Gillespie, A.R., 1995. Classification of multispectral images based on fractions of endmembers: applications to land-cover change in the Brazilian Amazon. Remote Sensing of Environment 52, 137–154.

Ali, M.M., Bayoumi, A.A.M.S., 2004. Assessment and mapping of desertification in western Sudan using remote sensing techniques and GIS. In: International Conf. on Water Resources and Arid Environment. PSIPW, Riyadh.

Anyamba, A., Tucker, C.J., 2005. Analysis of Sahelian vegetation dynamic using NOAA-AVHRR NDVI data from 1981–2003. Journal of Arid Environments 63, 596–614.

Asner, G.P., 2004. Biophysical remote sensing signatures of arid and semiarid ecosystem. In: Ustin, S.L. (Ed.), Remote Sensing for Natural Resources Management and Environmental Monitoring, third ed., Hoboken, New Jersey, pp. 53–109.

Ayoub, A.T., 1998. Extent, severity and causative factors of land degradation in the Sudan. Journal of Arid Environments 38, 397–409.

Bateson, C.A., Curtiss, B., 1996. A method for manual endmember selection and spectral unmixing. Remote Sensing of Environment 55, 229–243.

Bateson, C.A., Asner, G.P., Wessman, C.A., 2000. Endmember bundles: a new approach to incorporating endmember variability in spectral mixture analysis. IEEE Transactions on Geoscience and Remote Sensing 38, 1083–1094.

Brandt, J.S., Townsend, P.A., 2006. Land cover conversion, regeneration and degradation in the high elevation Bolivian Andes. Landscape Ecology 21, 607–623.

Chavez, P.S., 1988. An improved dark-object subtraction technique for atmospheric scattering correction of multispectral data. Remote Sensing of Environment 24, 459–479.

Collado, D.A., Chuvieco, E., Camarasa, A., 2002. Satellite remote sensing analysis to monitor desertification processes in the crop-rangeland boundary of Argentina. Journal of Arid Environments 52, 121–133.

Dafalla, M.S., Casplovics, E., 2005. Applicability and limitations of land use/land cover classification using high resolution satellite imagery in arid and semiarid areas of the Northern Kordofan State (Sudan). In: Roder, A., Hill, J. (Eds.), Proceedings of the First International Conference on Remote Sensing and Geoinformation Processing in the Assessment and Monitoring of Land Degradation and Desertification, Trier, Germany, pp. 549–555.

Dawelbait, M., Morari, F., 2008. Limits and potentialities of studying dryland vegetation using the optical remote sensing. Italian Journal of Agronomy 3, 97–106.

De Asis, A.M., Omasa, K., 2007. Estimation of vegetation parameter for modeling soil erosion using linear Spectral Mixture Analysis of Landsat ETM data. ISPRS Journal of Photogrammetry & Remote Sensing 62, 309–324.

Diouf, A., Lambin, E.F., 2001. Monitoring land cover changes in semiarid regions: remote sensing data and field observations in the Ferlo, Senegal. Journal of Arid Environments 48, 129–148.

Drake, N.A., White, K., 1991. Linear mixture modelling of Landsat Thematic Mapper data for mapping the distribution and abundance of gypsum in the Tunisian Southern Atlas, In Spatial data 2000. In: Dowman, I. (Ed.), Proceedings of a Joint Conference of the Photogrammetric Society, the Remote Sensing Society. The American Society for Photogrammetry and Remote Sensing, Christ Church, Oxford, pp. 168–177.

Eklundh, L., Olsson, L., 2003. Vegetation index trends for the African Sahel 1982–1999. Geophysical Research Letters 30, 1430.

Elmore, A.J., Mustard, J.F., Manning, S.J., Lobell, D.B., 2000. Quantifying vegetation change in semiarid environments. Remote Sensing of Environment 73, 87–102.

FAO-UNEP, 1984. Provisional Methodology for Assessment and Mapping of Desertification. FAO, Rome.

FAO-UNESCO, 1997. Soil Map of the World. Revised Legend, World Soil Resources Report 60, FAO, Rome. Reprinted with Updates as Technical Paper 20. ISRIC, Wageningen.

Hassan, H., Luscombe, W., 1990. Disaster information and technology transfer in developing countries. In: Kreimer, A., Munasinghe, M. (Eds.), Proceedings of the Colloquium on the Environment and Natural Disaster Management. World Bank, Washington, pp. 141–144.

Hellden, U., 2008. A coupled human-environment model for desertification simulation and impact studies. Global and Planetary Change 64, 158–168.

Le Houerou, H.N., 2006. Desertization. In: Lal, R. (Ed.), Soil Science. CRC Press, Boca Raton, Florida, pp. 468–474.

Huete, A.R., 1988. A soil-adjusted vegetation index (SAVI). Remote Sensing of Environment 25, 295–309.

Huete, A., 2004. Remote sensing of soil and soil processes. In: Ustin, S.L. (Ed.), Remote Sensing for Natural Resources Management and Environmental Monitoring, third ed. Hoboken, New Jersey, pp. 3–52.

Huete, A.R., van Leeuwen, W.J.D., Hua, G., Qi, J., Chehbouni, A., 1992. Normalization of multidirectional red and NIR reflectances with the SAVI. Remote Sensing of Environment 41, 143–154.

Jackson, R.D., Slater, P.N., Pinter, P.J., 1983. Discrimination of growth and water stress in wheat by various vegetation indices through clear and turbid atmospheres. Remote Sensing of Environment 13, 187–208.

Johnson, P.E., Smith, M.O., Adams, J.B., 1985. Quantitative analysis of planetary reflectance spectra with principal components analysis. Journal of Geophysical Research 90, C805–C810.

Khiry, M.A., 2007. Spectral Mixture Analysis for Monitoring and Mapping Desertification Processes in Semi-arid Areas, first ed. Rhombos-Verlag, Berlin.

Kuzera, K., Rogan, J., Eastman, J.R., 2005. Monitoring vegetation regeneration and deforestation using change vector analysis: MT. ST. Helens study area. In: ASPR 2005 Annual Conference Baltimore, Maryland.

Lillesand, T.M., Kiefer, R.W., Chipman, J.W., 2004. Remote Sensing and Image Interpretation, fifth ed. Las Vegas. New York.

Lu, D., Weng, Q., 2004. Spectral mixture analysis of the urban landscape in Indianapolis with Landsat ETM+ imagery. Photogrammetric Engineering & Remote Sensing 70, 1053–1062.

Mabbutt, J.A., 1986. Desertification indicators. Climatic Change 9, 113–122.

Malila, W.A., 1980. Change vector analysis: an approach for detecting forest changes with Landsat. In: Proceedings of the 6th Annual Symposium on Machine Processing of Remotely Sensed Data. Purdue University, West Lafayette, IN, pp. 326–335.

Markham, B.L., Barker, J.L., 1986. Landsat MSS and TM post-calibration dynamic ranges, exoatmospheric reflectances and at-satellite temperatures. EOSAT Landsat Technical Notes 1.
Moran, M.S., Bryant, R., Thome, K., Ni, W., Nouvellon, Y., Gonzalez-Dugo, M.P., Qi, J., 2001. A refined empirical line approach for reflectance factor retrieval from Landsat-5 TM and Landsat-7 ETM+. Remote Sensing of Environment 78, 71–82.
Mustafa, M.A., 2007. Desertification Processes, first ed. Khartoum University Press, Khartoum.
Nicholson, S., 2005. On the question of the "recovery" of the rains in the West African Sahel. Journal of Arid Environments 63, 615–641.
Okin, G.S., Robert, D.A., 2004. Remote sensing in arid regions: challenges and opportunities. In: Ustin, S.L. (Ed.), Remote Sensing for Natural Resources Management and Environmental Monitoring, third ed. Hoboken, New Jersey, pp. 111–145.
Qin, W., Gerstl, S.A.W., 2000. 3-D scene modelling of semi-desert vegetation cover and its radiation regime. Remote Sensing of Environment 74, 145–162.
Ray, T.W., Murray, B.C., 1996. Nonlinear spectral mixing in desert vegetation. Remote Sensing of Environment 55, 59–64.
Roberts, D.A., Smith, M.O., Adams, J.B., 1993. Green vegetation, non-photosynthetic vegetation, and soils in AVIRIS data. Remote Sensing of Environment 44, 255–269.
Rubio, J.L., Bochet, E., 1998. Desertification indicators as diagnosis criteria for desertification risk assessment in Europe. Journal of Arid Environments 39, 113–120.
Scaramuzza, P., Micijevic, E., Chander, G., 2004. SLC gap-filled products phase one methodology. Landsat Technical Notes.
Sherbinin, D.S., 2002. A CIESIN Thematic Guide to Land-use and Land-cover Change (LUCC). Columbia University, Palisades, NY.
Singh, G., 2009. Salinity-related desertification and management strategies: Indian experience. Land Degradation & Development 20, 367–385.
Small, C., 2001. Estimation of urban vegetation abundance by spectral mixture analysis. International Journal of Remote Sensing 22, 1305–1334.
Small, C., 2004. The Landsat ETM+ spectral mixing space. Remote Sensing of Environment 93, 1–17.
Smith, M.O., Johnson, P.E., Adams, J.B., 1985. Quantitative determination of mineral types and abundances from reflectance spectra using principal components analysis. Journal of Geophysical Research 90, C797–C804.
Smith, M.O., Ustin, S.L., Adams, J.B., Gillespie, A.R., 1990. Vegetation in deserts: I. A regional measure of abundance from multispectral images. Remote Sensing of Environment 31, 1–26.
Theseira, M.A., Thomas, G., Taylor, J.C., Gemmell, F., Varjo, J., 2003. Sensitivity of mixture modelling to endmember selection. International Journal of Remote Sensing 24, 1559–1575.
Tilahun, K., 2006. Analysis of rainfall climate and evapo-transpiration in arid and semi-arid regions of Ethiopia using data over the last half a century. Journal of Arid Environment 64, 474–487.
Tompkins, S., Mustard, J.F., Pieters, C.M., Forsyth, D.W., 1997. Optimization of end-members for spectral mixture analysis. Remote Sensing of Environment 59, 472–489.
Trodd, N.M., Dougill, A.J., 1998. Monitoring vegetation dynamics in semi-arid African rangelands. Applied Geography 18, 315–330.
Tucker, C.J., 1979. Red and photographic infrared linear combinations for monitoring vegetation. Remote Sensing of Environment 8, 127–150.
Tueller, P.T., Oleson, S.G., 1989. Diurnal radiance and shadow fluctuations in a cold desert shrub plant community. Remote Sensing Environment 29, 1–13.
UNCCD, 1994. Status of Ratification and Entry into Force. United Nations Convention to Combat Desertification Paris.
UNEP, 2007. Sudan Post-Conflict Environmental Assessment. United Nations Environment Programme, Geneva.
Villeneuve, P.V., Gerstl, S.A., Asner, G.P., 1998. Estimating nonlinear mixing effects for arid vegetation scenes with MISR channels and observation directions. In: CH 36042 (Ed.), 1998. Proceedings of the International Geoscience and Remote Sensing Symposium. Singapore, vol. 3, pp. 31–35.
Wessman, C.A., Bateson, C.A., Benning, T.L., 1997. Detecting fire and grazing patterns in tallgrass prairie using spectral mixture analysis. Ecological Applications 7, 493–512.
Wu, C., 2004. Normalization spectral mixture analysis for monitoring urban composition using ETM+ imagery. Remote Sensing of Environment 93, 480–492.